Relativistic Brueckner-Hartree-Fock theory in nuclear matter without the average momentum approximation

Hui Tong (童辉),[1] Xiu-Lei Ren (任修磊),[1,2] Peter Ring,[1,3] Shi-Hang Shen (申时行),[1]
Si-Bo Wang (王锶博),[1] and Jie Meng (孟杰)[1,4,5,*]

[1]*State Key Laboratory of Nuclear Physics and Technology, School of Physics, Peking University, Beijing 100871, China*
[2]*Institut für Theoretische Physik II, Ruhr-Universität Bochum, D-44780 Bochum, Germany*
[3]*Physik-Department der Technischen Universität München, D-85748 Garching, Germany*
[4]*Department of Physics, University of Stellenbosch, Stellenbosch, South Africa*
[5]*Yukawa Institute for Theoretical Physics, Kyoto University, Kyoto 606-8502, Japan*

(Received 28 August 2018; published 5 November 2018)

Brueckner-Hartree-Fock theory allows one to derive the G matrix as an effective interaction between nucleons in the nuclear medium. It depends on the center-of-mass momentum $\boldsymbol{P}$ of the two particles and on the two relative momenta $\boldsymbol{q}$ and $\boldsymbol{q}'$ before and after the scattering process. In the evaluation of the total energy per particle in nuclear matter, usually the angle-averaged center-of-mass momentum approximation has been used. We derive in detail the exact expressions of the angular integrations of the momentum $\boldsymbol{P}$ within relativistic Brueckner-Hartree-Fock (RBHF) theory, especially for the case of asymmetric nuclear matter. In order to assess the reliability of the conventional average momentum approximation for the binding energy, the saturation properties of symmetric and asymmetric nuclear matter are systematically investigated based on the realistic Bonn nucleon-nucleon potential. It is found that the exact treatment of the center-of-mass momentum leads to non-negligible contributions to the higher order physical quantities. The correlations between the symmetry energy $E_{\rm sym}$, the slope parameter L, and the curvature $K_{\rm sym}$ of the symmetry energy are investigated. The results of our RBHF calculations for the bulk parameters characterizing the equation of state are compared with recent constraints extracted from giant monopole resonance and isospin diffusion experiments.

DOI: 10.1103/PhysRevC.98.054302

I. INTRODUCTION

The investigation of the nuclear equation of state (EoS), especially its properties under extreme conditions, is one of the most crucial issues in both nuclear physics and astrophysics. It is important to understand a variety of interesting phenomena including supernova explosions, the mass-radius correlations of neutron stars, the collective motion of nucleons within the nuclei, the neutron skin thickness of heavy nuclei, as well as some other topics [1–8]. In recent years, with the establishment of many facilities for radioactive ion beams in terrestrial laboratories, such as the Cooling Storage Ring (CSR) Facility in China, the Radioactive Ion Beam (RIB) Factory at RIKEN in Japan, the GSI Facility for Antiproton and Ion Research (FAIR) in Germany, SPIRAL2 at the Grand Accelerateur National d'Ions Lourds (GANIL) in France, and the Facility for Rare Isotope Beams (FRIB) in the United States, it has become possible to explore experimentally the EoS of nuclear matter at large isospin asymmetry; in particular, the density dependence of the nuclear symmetry energy.

Theoretical models which are used to investigate the properties of the nuclear EoS can roughly be divided into two methods: phenomenological and *ab initio* methods. Phenomenological methods, either nonrelativistic or relativistic, are based on density functionals such as Skyrme [9,10], Gogny [11], or relativistic mean-field (RMF) models [12–16] that are constructed for the purpose of reproducing properties of finite nuclei and nuclear matter. *Ab initio* methods are based on realistic nucleon-nucleon (NN) interactions with nuclear many-body techniques used for a microscopic treatment of the nuclear system.

There are a variety of formulations of the NN interactions, such as Bonn [17], AV18 [18], CD Bonn [19], and chiral potentials [20–23]. Recently, more and more *ab initio* methods have been developed to study the nuclear many-body system; these include the quantum Monte Carlo method [24], the coupled-cluster method [25], the no-core shell model [26], the self-consistent Green's function method [27], the lattice chiral effective field theory [28], the in-medium similarity renormalization group [29], the Monte Carlo shell model [30,31], and the Brueckner-Hartree-Fock (BHF) theory [32]. Among these, the relativistic Bonn potential has been successfully applied in relativistic Brueckner-Hartree-Fock (RBHF) theory [33], to study both nuclear matter [34–42] and, more recently, finite nuclei [43–47].

Comparing with nonrelativistic BHF, RBHF theory in nuclear matter is relatively complicated and time-consuming. Therefore, in order to reduce the complexity of this method, in the earlier investigations the so called average center-of-mass (c.m.) momentum approximation was used for the calculation of the binding energy per particle [40,48–50]. With the rapid

*mengj@pku.edu.cn

increase of computational power, however, it is now possible to avoid this approximation. In the present work we derive exact and analytic formulations of the angular integrations for the c.m. momentum $\boldsymbol{P}$ in the framework of RBHF theory, especially for asymmetric nuclear matter. In addition, we systematically study both the density dependence of the energy in symmetric nuclear matter and the symmetry energy at the saturation density ρ_0. For the calculations we use the Bonn potentials [17] and compare results with and without the averaged c.m. momentum approximation. In particular we examine the effect of the exact treatment of the c.m. momentum for the higher order physical quantities in both the energy in symmetric nuclear matter and the symmetry energy.

In Sec. II, we will first describe the general properties of nuclear matter, and then give a brief review of the RBHF framework. Next, we will derive an exact and analytic expression of the angular integrations for the c.m. momentum $\boldsymbol{P}$. Results and discussions are presented in Sec. III and a summary is finally given in Sec. IV.

II. THEORETICAL FRAMEWORK

A. Saturation properties of nuclear matter

The binding energy per nucleon of isospin asymmetric nuclear matter can be generally expressed as a power series in the asymmetry parameter $\alpha = (\rho_n - \rho_p)/\rho$, where $\rho = \rho_n + \rho_p$ is the total density with ρ_n and ρ_p expressing the neutron and proton densities:

$$E(\rho,\alpha) = E(\rho,0) + E_{\rm sym}(\rho)\alpha^2 + O(4). \tag{1}$$

Here $E(\rho,0)$ is the binding energy per nucleon of symmetric nuclear matter and $E_{\rm sym}(\rho)$ is the so-called nuclear symmetry energy,

$$E_{\rm sym}(\rho) = \frac{1}{2}\frac{\partial^2 E(\rho,\alpha)}{\partial\alpha^2}\bigg|_{\alpha=0}. \tag{2}$$

The binding energy per nucleon in symmetric nuclear matter can be expanded around the saturation density ρ_0,

$$E(\rho,0) = E(\rho_0,0) + \frac{K_\infty}{2}\left(\frac{\rho-\rho_0}{3\rho_0}\right)^2 + \frac{Q_0}{6}\left(\frac{\rho-\rho_0}{3\rho_0}\right)^3 + O(4), \tag{3}$$

where $E(\rho_0,0)$ denotes the binding energy per nucleon. The second and third derivatives of $E(\rho,0)$ with respect to ρ are given by the incompressibility $K(\rho)$ and the skewness parameter $Q(\rho)$,

$$K(\rho) = 9\rho_0^2\frac{\partial^2 E(\rho,0)}{\partial\rho^2}, \tag{4}$$

$$Q(\rho) = 27\rho_0^3\frac{\partial^3 E(\rho,0)}{\partial\rho^3}, \tag{5}$$

and K_∞ and Q_0 are their values at the saturation density ρ_0, respectively. The slope of the nuclear matter incompressibility is given by [51]

$$M(\rho) = 3\rho\frac{\partial K(\rho)}{\partial\rho}, \tag{6}$$

and, at saturation density, we find

$$M_0 = M(\rho_0) = 12K_\infty + Q_0. \tag{7}$$

In Ref. [52], the investigation of these quantities shows a strong correlation of the neutron star radii with the slope of the incompressibility.

Similarly, in the vicinity of the saturation density ρ_0, the symmetry energy can also be characterized in terms of a few bulk parameters:

$$E_{\rm sym}(\rho) = E_{\rm sym}(\rho_0) + L\left(\frac{\rho-\rho_0}{3\rho_0}\right) + \frac{K_{\rm sym}}{2}\left(\frac{\rho-\rho_0}{3\rho_0}\right)^2 + O(3), \tag{8}$$

where $E_{\rm sym}(\rho_0)$ is the value of the symmetry energy at saturation density and L and $K_{\rm sym}$ are the slope parameter and curvature parameter of the nuclear symmetry energy at ρ_0:

$$L = 3\rho_0\frac{\partial E_{\rm sym}(\rho)}{\partial\rho}\bigg|_{\rho=\rho_0}, \tag{9}$$

$$K_{\rm sym} = 9\rho_0^2\frac{\partial^2 E_{\rm sym}(\rho)}{\partial\rho^2}\bigg|_{\rho=\rho_0}. \tag{10}$$

The nuclear matter incompressibility K_∞ is not a directly measurable quantity. Instead, one can also define an incompressibility K_A for a finite nucleus with mass number A by measuring the excitation energy of the isoscalar giant monopole resonance (ISGMR) [53],

$$E_{\rm ISGMR} = \sqrt{\frac{\hbar^2 K_A}{M\langle r^2\rangle}}, \tag{11}$$

where M is the nucleon mass and $\langle r^2\rangle$ is the mean square radius of the ground state. This incompressibility for finite nuclei can be parametrized by means of a similar expansion to the liquid drop mass formula with volume, surface, symmetry, and Coulomb terms [53]:

$$K_A \approx K_\infty + K_{\rm surf}A^{-1/3} + K_\tau\alpha^2 + K_{\rm Coul}\frac{Z^2}{A^{4/3}}. \tag{12}$$

The symmetry term K_τ and the Coulomb term $K_{\rm Coul}$ are related to nuclear matter properties as [53–56]

$$K_\tau = K_{\rm sym} - 6L - \frac{Q_0}{K_\infty}L, \tag{13}$$

$$K_{\rm Coul} = \frac{3}{5}\frac{e^2}{r_0}\left(-8 - \frac{Q_0}{K_\infty}\right), \tag{14}$$

where r_0 is the radius constant defined by

$$r_0 = \left(\frac{3}{4\pi\rho_0}\right)^{1/3}. \tag{15}$$

If one uses the parabolic approximation in Eq. (3) ($Q_0 = 0$), then K_τ can be simplified to

$$K_\tau \approx K_{\rm asy} = K_{\rm sym} - 6L. \tag{16}$$

This equation has been widely used to characterize the isospin dependence of the incompressibility of asymmetric nuclear

matter in Refs. [6–8,57–60]. Obviously, if the skewness parameter Q_0 is negligible or the magnitude of the slope parameter L is very small, then the coefficient $K_{\rm asy}$ could be a good approximation to K_τ. Therefore it is important to study in a microscopic approach how the term Q_0 affects the value of K_τ.

As mentioned before, in this investigation we use RBHF theory. In the following, the concepts of this theory in nuclear matter will be briefly reviewed.

B. Relativistic Brueckner-Hartree-Fock theory

To evaluate the in-medium nucleon-nucleon potential, one needs a Dirac spinor which is the solution of the Dirac equation for the description of the single-particle motion in the nuclear medium,

$$u_\tau(\boldsymbol{p}, s) = \left(\frac{E^*_\tau(p) + M^*_\tau}{2E^*_\tau}\right)^{1/2} \begin{pmatrix} 1 \\ \frac{\boldsymbol{\sigma}\cdot\boldsymbol{p}}{E^*_\tau(p)+M^*_\tau} \end{pmatrix} \chi_s. \tag{17}$$

Here $M^*_\tau = M + U_{S,\tau}$ and $E^{*2}_\tau(p) = M^{*2}_\tau + \boldsymbol{p}^2$. $U_{S,\tau}$ denotes the scalar potential. τ is the isospin quantum number, and χ_s a Pauli spinor. The normalization is $u^\dagger_\tau(\boldsymbol{p}, s)u_\tau(\boldsymbol{p}, s) = 1$.

One of the most widely used equations in the RBHF approach is the Thompson equation [61], which is a relativistic three-dimensional reduction of the Bethe-Salpeter equation [62]. The in-medium Thompson equation describes the scattering of two nucleons in nuclear matter. It allows one to derive the G matrix as an effective interaction in the medium from the solution of the following equation in the momentum space:

$$\begin{aligned} &G_{\tau_1\tau_2}\big(\boldsymbol{q}', \boldsymbol{q}\big|\boldsymbol{P}, W_{\tau_1\tau_2}\big) \\ &\quad = V_{\tau_1\tau_2}(\boldsymbol{q}', \boldsymbol{q}) + \int \frac{d^3k}{(2\pi)^3}\, V_{\tau_1\tau_2}(\boldsymbol{q}', \boldsymbol{k}) \\ &\qquad \times \frac{Q_{\tau_1\tau_2}(\boldsymbol{k}, \boldsymbol{P})}{W_{\tau_1\tau_2} - E^*_{\tau_1\tau_2}} G_{\tau_1\tau_2}\big(\boldsymbol{k}, \boldsymbol{q}\big|\boldsymbol{P}, W_{\tau_1\tau_2}\big), \end{aligned} \tag{18}$$

where $\tau_1\tau_2 = nn$, pp, or np. $V_{\tau_1\tau_2}$ denotes a realistic bare nucleon-nucleon interaction [17] and it is constructed in terms of effective Dirac states (in-medium spinors) as explained in Eq. (17). Equation (18) deviates from the Thompson equation (6) in Ref. [35] by the factor M^2/E^2, because we use the Dirac spinors (17) normalized according to $u^\dagger u = 1$, as is usual in many-body physics (see for instance Serot and Walecka in Ref. [63]). $W_{\tau_1\tau_2}$ is the starting energy and $E^*_{\tau_1\tau_2}$ is the total energy of intermediate two-nucleon states. $\boldsymbol{P}$ is the c.m. momentum and $\boldsymbol{q}$, $\boldsymbol{q}'$, and $\boldsymbol{k}$ are the initial, final, and intermediate relative momenta,

$$\boldsymbol{P} = \frac{\boldsymbol{k_1} + \boldsymbol{k_2}}{2}, \tag{19}$$

$$\boldsymbol{k} = \frac{\boldsymbol{k_1} - \boldsymbol{k_2}}{2}. \tag{20}$$

The momenta of the two interacting particles $\boldsymbol{k_1}$ and $\boldsymbol{k_2}$ in nuclear matter can be expressed in terms of the relative momentum $\boldsymbol{k}$ and the c.m. momentum $\boldsymbol{P}$. The Pauli operator $Q_{\tau_1\tau_2}(\boldsymbol{k}, \boldsymbol{P})$ avoids the scattering into occupied states, i.e., into states with $|\boldsymbol{k_1}| \leqslant k_F^{\tau_1}$ or $|\boldsymbol{k_2}| \leqslant k_F^{\tau_2}$. It is defined as

$$Q_{\tau_1\tau_2}(\boldsymbol{k}, \boldsymbol{P}) = \begin{cases} 1, & |\boldsymbol{P} + \boldsymbol{k}| > k_F^{\tau_1} \text{ or } |\boldsymbol{P} - \boldsymbol{k}| > k_F^{\tau_2}, \\ 0, & \text{otherwise.} \end{cases} \tag{21}$$

where $Q_{\tau_1\tau_2}(\boldsymbol{k}, \boldsymbol{P})$ depends not only on the magnitude of the c.m. and relative momenta but also on their relative directions. To simplify such an angular dependence, one usually replaces the Pauli operator $Q_{\tau_1\tau_2}(\boldsymbol{k}, \boldsymbol{P})$ by an angle-averaged Pauli operator $Q^{\rm av}_{\tau_1\tau_2}(k, P)$ [see Eq. (A1) in Appendix A]. Several nonrelativistic investigations have been carried out to calculate the nuclear matter properties using the exact Pauli operator $Q_{\tau_1\tau_2}(\boldsymbol{k}, \boldsymbol{P})$, and almost all the results have assessed the reliability of this angle-averaged approximation in the nonrelativistic framework [64–66]. Therefore we use this approximation also in the relativistic case. For asymmetric nuclear matter this value has to be carefully investigated, and the details are given in the Appendix A.

After the solution of Eq. (18) for the positive energy solutions, the knowledge of the G matrix allows us to calculate the self energy:

$$U_{\tau_1}(m) = \sum_{s_n,\tau_2} \frac{1}{(2\pi)^3} \int_0^{k_F^{\tau_2}} d^3k_n \langle mn|G_{\tau_1\tau_2}(W_{\tau_1\tau_2})|mn - nm\rangle, \tag{22}$$

for the positive energy solutions. Here m specifies a state below or above the Fermi surface with momentum $\boldsymbol{k}_m$ and spin s_m. $W_{\tau_1\tau_2}$ is the starting energy and we use in the following calculations the "continuous choice" [67,68],

$$W_{\tau_1\tau_2} = E^*_{\tau_1}(p_m) + E^*_{\tau_1}(p_n). \tag{23}$$

Before solving the relativistic Hartree-Fock equations in a self-consistent way, one needs the full relativistic single-particle potential $U(p)$ and the full self-energy, i.e., matrix elements not only for the positive energy solutions given in Eq. (22), but also the elements coupling positive with negative energy solutions and those for the negative with negative energy solutions. Following the usual prescriptions [35,49], where the Thompson equation is solved only for the positive energy solutions, and neglecting the spacelike component of the vector field because of time-reversal invariance, we use the following ansatz for the single-particle potential:

$$U(p) = U_S + \gamma_0 U_V. \tag{24}$$

Furthermore, the momentum dependence of the scalar and vector fields is very weak and neglected. The two constants U_S and U_V are adjusted to the positive energy solutions in Eq. (22) at the Fermi momentum. This leads to the relativistic Hartree-Fock equation

$$\{\boldsymbol{\alpha}\cdot\boldsymbol{p} + U_V + \beta M^*\}u(\boldsymbol{p}) = E(p)u(\boldsymbol{p}), \tag{25}$$

where $\boldsymbol{\alpha} = \gamma_0\boldsymbol{\gamma}$ and $\beta = \gamma_0$ are the Dirac matrices, $M^* = M + U_S$ is the effective mass, and $u(\boldsymbol{p})$ are the Dirac spinors given in Eq. (17). The eigenvalues $E(p) = U_V + E^*(p)$ are used for the solution of the Thompson equation (18) in the next step of the iteration.

Considering the isospin dependence, it is evident that U_n and U_p in Eq. (22) are coupled through the np component of

the potential:

$$U_n = U_{nn} + U_{np}, \tag{26}$$

$$U_p = U_{pp} + U_{pn}. \tag{27}$$

Therefore they must be solved simultaneously, and the relativistic $G_{\tau_1\tau_2}$ matrix is self-consistently evaluated with the single-particle potentials and the single-particle energies in the standard RBHF iterative procedure. Once the solution has converged, the total energy per nucleon in nuclear matter can be calculated by [35]

$$\frac{E}{A} = \frac{1}{A}\sum_{s_m,\tau}\frac{1}{(2\pi)^3}\int_0^{k_F^\tau} d^3k_m \langle m|\boldsymbol{\alpha}\cdot\boldsymbol{k}_m + \beta M|m\rangle - M + \frac{1}{2A}\sum_{s_m,s_n,\tau_1,\tau_2}\frac{1}{(2\pi)^6}\int_0^{k_F^{\tau_1}} d^3k_m \int_0^{k_F^{\tau_2}} d^3k_n \langle mn|G_{\tau_1\tau_2}\big(W_{\tau_1\tau_2}\big)|mn-nm\rangle. \tag{28}$$

As mentioned above, we will focus on the calculation of the potential energy.

C. Potential energy

As previously mentioned, the G matrix is directly obtained from the Thompson equation (18) which is written in the c.m. frame of the two scattering nucleons. Thus, Eq. (28) should be transformed to the c.m. frame. This yields for the potential energy, the second line of Eq. (28),

$$\frac{E_V}{A} = \frac{1}{2\rho}\frac{8}{(2\pi)^3}\sum_{mn}\int^{(k_F^{\tau_1}+k_F^{\tau_2})/2} d^3q \int^{\substack{|\boldsymbol{q}+\boldsymbol{P}|\leqslant k_F^{\tau_1}\\ |\boldsymbol{q}-\boldsymbol{P}|\leqslant k_F^{\tau_2}}} d^3P \langle \boldsymbol{q}mn|G_{\tau_1\tau_2}\big(\boldsymbol{P}, W_{\tau_1\tau_2}\big)|\boldsymbol{q}mn-nm\rangle, \tag{29}$$

with the total density $\rho = \rho_n + \rho_p$ and the momenta $\boldsymbol{P} = (\boldsymbol{k_m} + \boldsymbol{k_n})/2$, $\boldsymbol{q} = (\boldsymbol{k_m} - \boldsymbol{k_n})/2$. The factor 8 is caused by the transformation from the laboratory frame to the c.m. frame. The integral over the c.m. momentum $\boldsymbol{P}$ in Eq. (29) cannot be performed separately because of the momentum dependence of the G matrix. Obviously, the angular integrations $\int d\Omega_P$ in $\int d^3P$ depends not only on the magnitude of the total and the relative momenta but also on their relative directions.

In the literatures, the averaged c.m. momentum approximation has been used [40,48], where the average c.m. momentum is defined as

$$P^2_{\rm av} = \frac{\int_0^{k_F^n} d^3k_1 \int_0^{k_F^p} d^3k_2 P^2 \delta\big(q - \frac{1}{2}|\boldsymbol{k}_1 - \boldsymbol{k}_2|\big)}{\int_0^{k_F^n} d^3k_1 \int_0^{k_F^p} d^3k_2 \delta\big(q - \frac{1}{2}|\boldsymbol{k}_1 - \boldsymbol{k}_2|\big)}. \tag{30}$$

It does not depend on the direction, and this value is usually applied in the G matrix in Eq. (29) (for further details see Appendix C).

In this investigation we do not use this approximation and we focus here on how to carry out the angular integrations $\int d\Omega_P = \int \sin\theta\, d\theta\, d\phi$ exactly, where θ is the angle between $\boldsymbol{q}$ and $\boldsymbol{P}$. On the basis of the conditions $|\boldsymbol{k_m}| = |\boldsymbol{P} + \boldsymbol{q}| \leqslant k_F^{\tau_1}$ and $|\boldsymbol{k_n}| = |\boldsymbol{P} - \boldsymbol{q}| \leqslant k_F^{\tau_2}$, this leads to restrictions on the angle θ. First, in order to give a clearer understanding of the calculations in detail, the Fermi sphere method [69] is adopted as a powerful tool to calculate the angle integral $\int d\Omega_P$ in Eq. (29). Assuming $k_F^n \geqslant k_F^p$, since the range of $|\boldsymbol{q}|$ is strongly affected by the comparison between the values of k_F^p and $(k_F^n - k_F^p)/2$, i.e., by the relation between k_F^n and $3k_F^p$, one has to distinguish two cases:

$$\text{(a)}\quad k_F^n \geqslant 3k_F^p \quad (\text{or } \alpha \geqslant 13/14), \tag{31}$$

$$\text{(b)}\quad k_F^n \leqslant 3k_F^p \quad (\text{or } \alpha \leqslant 13/14), \tag{32}$$

with the asymmetry parameter $\alpha = (\rho_n - \rho_p)/\rho = ({k_F^n}^3 - {k_F^p}^3)/({k_F^n}^3 + {k_F^p}^3)$. Moreover, there exist three possible situations depending on the value of $|\boldsymbol{q}|$ in both of the cases (a) and (b), and a more complicated problem is that at a given $|\boldsymbol{q}|$, there are also several regions depending on the magnitude of $|\boldsymbol{P}|$. The details and the results of the exact angular integration $\int d\Omega_P$ in Eq. (29) are provided in Appendix B.

III. RESULTS AND DISCUSSION

We summarize our results for the properties of nuclear matter in Table I. In the first row, we show our RBHF results with (average) and without (exact) the approximation of averaged c.m. momentum. The nonrelativistic BHF results with and without three-body forces (TBF) are shown in the second row. For comparison, empirical values are also listed.

In comparison with the results from nonrelativistic BHF calculations without three-body forces, the saturation point is shifted towards lower density for relativistic BHF theory using the Bonn potentials. The result for potential Bonn A even meets the empirical region [70,71]. In order to reproduce the saturation point of symmetric nuclear matter within nonrelativistic BHF, one needs to introduce a three-body force in Ref. [72]. This three-body force requires two phenomenological parameters that need to be fixed by requiring that the BHF calculation reproduce the energy and saturation density of symmetric nuclear matter. In Table I, two sets of such parameters are presented: the original set of Ref. [73] (labeled TBFa), and another new set of Ref. [72] (labeled TBFb), in which the parameter associated with the two-pion attractive term has been reduced by 10%, and the one associated with the phenomenological repulsive term has been increased by 20% in order to get a smaller saturation density.

TABLE I. Bulk parameters (as described in the text) of symmetric and asymmetric nuclear matter at saturation density ρ_0. Results obtained in RBHF theory using the Bonn potentials A, B, and C with exact and averaged c.m. momentum are compared with those found in nonrelativistic BHF theory with and without TBF [35,72,74]. The quantities Δ are defined as the differences between the exact and the averaged treatments of the c.m. momentum. The empirical values are also listed in the last row.

Model	Potential		ρ_0 (fm^{-3})	E/A (MeV)	K_∞ (MeV)	Q_0 (MeV)	M_0 (MeV)	E_{sym} (MeV)	L (MeV)	K_{sym} (MeV)	K_{asy} (MeV)	K_τ (MeV)	K_{Coul} (MeV)
RBHF	A	exact	0.180	−15.38	286	731	4163	33.7	75.8	−57.0	−512	–705	–8.30
		average	0.182	−15.04	289	650	4118	32.6	74.7	−53.1	−501	–669	–8.09
		Δ	−0.002	−0.34	–3	81	45	1.1	1.1	−3.9	−11	–36	–0.21
	B	exact	0.164	−13.44	222	547	3211	29.9	63.0	−56.3	−434	–590	–7.98
		average	0.165	−13.08	220	791	3431	28.7	65.3	−47.5	−439	–674	–8.86
		Δ	−0.001	−0.36	2	–244	–220	1.2	−2.3	−8.8	5	84	0.88
	C	exact	0.149	−12.12	176	260	2372	26.8	51.7	−55.6	−366	–442	–7.00
		average	0.150	−11.75	168	638	2654	25.6	58.8	−41.1	−394	–618	–8.74
		Δ	−0.001	−0.37	8	–378	–282	1.2	−7.1	−14.5	28	176	1.74
BHF	A		0.428	−23.55	204			32.1					
	B		0.309	−18.30	160			31.8					
	C		0.247	−15.75	143			28.5					
	AV18	without TBF	0.240	−17.30	214	–225	2343	35.8	63.1	−27.8	−406	–340	–6.01
	AV18	TBFa	0.187	−15.23	196	–281	2071	34.3	66.5	−31.3	−430	–335	–5.23
	AV18	TBFb	0.176	−14.62	186	–225	2007	33.6	66.9	−23.4	−425	–344	–5.30
Empirical			0.166 ±0.018	−16 ±1	240 ±20			32 ±2	88 ±25			–550 ±100	

In the sixth column of Table I we show the symmetry energy at saturation density. For the exact calculation it turns out to be 33.7 MeV, which is in good agreement with the empirical value of 32 ± 2 MeV [5].

Using the previously discussed RBHF method, the incompressibility of nuclear matter at saturation density is 286 MeV for the potential Bonn A and about 222 MeV for the potential Bonn B, which is in satisfactory agreement with the commonly accepted value of 240 ± 20 MeV [56,75,76]. It should be noted that, after including the three-body forces within nonrelativistic BHF, the incompressibility coefficient decreases considerably and reaches values far from the lower bound of $K_\infty = 220$ MeV imposed by experiments. It should be mentioned here that the comparison of these two incompressibilities is influenced by the fact that they are calculated at different saturation densities.

At present, there is no experimental constraint on Q_0, which is defined as the third density derivative of the symmetric nuclear matter energy at saturation. The microscopic predictions of RBHF theory for Q_0 are large and positive, in contrast to the nonrelativistic BHF results with negative values. As a consequence, in Eq. (14) the values of $K_{\mathrm{Coul}} = \frac{3}{5}\frac{e^2}{r_0}(-8 - \frac{Q_0}{K_\infty})$ are larger for RBHF than those found in nonrelativistic BHF. We also see that the approximate expression (16) $K_\tau \approx K_{\mathrm{asy}} = K_{\mathrm{sym}} - 6L$ [7,8,58], which is quite often used instead of $K_\tau = K_{\mathrm{asy}} - (Q_0/K_\infty)L$, can lead to a remarkable difference in K_τ. The results of this addendum indicate that generally the higher order Q_0 contribution to K_τ cannot be neglected, either in relativistic or in non-relativistic BHF, especially for larger L values.

It is shown that the saturation densities do not change substantially for the exact treatment of the c.m. momentum given in Appendix B as compared to the results of the averaged c.m. momentum approximation in Appendix C. It is a common characteristic of the results for the three different nucleon-nucleon potentials (Bonn A, B, and C) that the exact treatment of the c.m. momentum produces small but non-negligible contributions to the binding energy per nucleon at saturation densities, as compared with the results of the conventional averaged c.m. momentum approximation. These non-negligible differences in the binding energy are important when studying effects of higher order physical quantities in both the energy in symmetric nuclear matter and the symmetry energy. For some of the properties associated with the EoS, such as ρ_0, E/A, K_∞, E_{sym}, and L, the differences are relatively small, but they become significant for the remaining higher order parameters. Especially we find significant differences for the quantities Q_0, M_0, K_{sym}, K_{asy}, K_{Coul}, and K_τ.

In order to have accurate expressions for the various quantities defined as the density derivatives of the energy of symmetric nuclear matter and of the symmetry energy in Table I, we parametrized the energy of symmetric nuclear matter and the symmetry energy in the vicinity of the saturation density ρ_0. It has been found that the EoS can be accurately represented using the following functional form [77]:

$$\frac{E}{A}(\rho) = a\left(\frac{\rho}{\rho_0}\right)^\alpha + b\left(\frac{\rho}{\rho_0}\right)^\beta, \tag{33}$$

where E/A is the binding energy per nucleon as a function of the nuclear density ρ, and the parameters a, α, b, and β are obtained by fitting to the results of RBHF theory for the different Bonn potentials. In a similar way, a two-parameter representation for the symmetry energy around saturation

TABLE II. Fit parameters for the nuclear matter properties defined in Eqs. (33) and (34) for RBHF theory using the Bonn potentials A, B, and C.

Model	Potential		a (MeV)	α	b (MeV)	β	c (MeV)	γ
RBHF	A	exact	−19.25	0.64	3.87	3.21	33.72	0.75
		average	−19.53	0.70	4.49	3.05	32.63	0.76
	B	exact	−16.23	0.56	2.79	3.26	29.92	0.70
		average	−15.15	0.51	2.07	3.69	28.73	0.76
	C	exact	−14.89	0.55	2.77	2.94	26.85	0.64
		average	−13.15	0.41	1.40	3.86	25.57	0.77

density is frequently used [7]:

$$E_{\rm sym}(\rho) = c\left(\frac{\rho}{\rho_0}\right)^{\gamma}. \tag{34}$$

The results of these fits, i.e., the parametrization of the equations of state obtained with and without c.m. momentum approximation, are shown in Table II and in Fig. 1. Of course, a fit of a given function does not guarantee that the derivative of the fit is itself a good fit of the numerical derivative. Therefore, in order to ensure the current results are reliable, we also made numerical derivatives and we found that the errors between the two methods were less than 5%, even for the third order.

As we can see in Fig. 1, the binding energy calculated by RBHF theory using the potential Bonn A without the c.m. momentum approximation agrees better with the empirical value than the results based on the c.m. momentum approximation.

In Fig. 2 we show the correlations between L and $E_{\rm sym}$ (left panel) and between L and $K_{\rm sym}$ (right panel), which have been investigated in Refs. [72,80]. The values of $E_{\rm sym}$ and $K_{\rm sym}$ obtained from both the nonrelativistic (squares) and relativistic (circles) density functionals exhibit a linear correlation with L. It should be mentioned that the result of RBHF theory using the potential Bonn A is in excellent agreement with this tight correlation. In addition, other *ab initio* calculations, such as the results of nonrelativistic BHF and the variational microscopic calculations of Akmal, Pandharipande, and Ravenhall (hereafter APR) which incorporate relativistic boost corrections and three-nucleon interactions (using the A18+δv + UIX* interaction) [78] are also given. It can be seen that these two correlations also exist in microscopic approaches. Note that the RBHF results for L are also located inside the region constrained by the isospin diffusion data [7,58,80]. According to Fig. 2, it is clear that the symmetry energy $E_{\rm sym}$ and the curvature parameter $K_{\rm sym}$ are both sensitive to the slope parameter L, increasing almost linearly with increasing L. There is no direct experimental information on the $K_{\rm sym}$ parameter. However, as proposed in Ref. [81], once accurate experimental information becomes available for L, these correlations could be exploited to obtain theoretical estimates for $K_{\rm sym}$.

One can see in Fig. 3 the values of K_∞, L, and K_τ for the present RBHF calculations using the Bonn potentials, compared with the predictions of BHF and APR as given in Table I. The shaded rectangular regions encompass the recent values of $K_\infty = 240 \pm 20$ MeV [56,75], $K_\tau = -550 \pm 100$ MeV [56,75], and $L = 88 \pm 25$ MeV [7,58,80]. The experimental values obtained from the ISGMR and from isospin diffusion for K_τ, K_∞, and L together provide a way to choose the most appropriate interaction used in the EoS calculations. Although a majority of the interactions fail to meet the regions established by these measurements, it is worth mentioning here that the results of RBHF theory using the potential Bonn B without c.m. momentum approximation lie within this

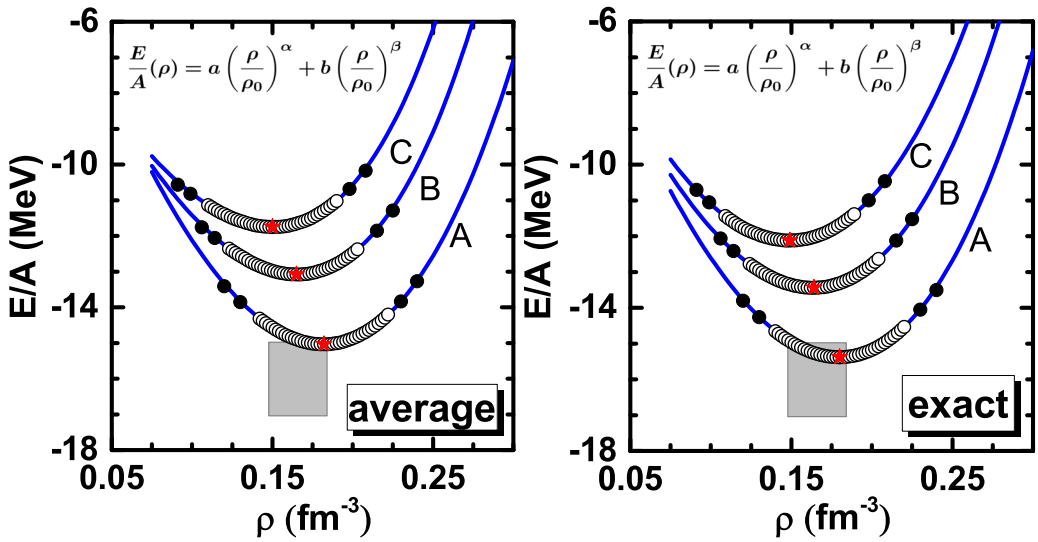

FIG. 1. Binding energy per nucleon for nuclear matter as a function of the total density ρ. Results for Bonn potentials A, B, C with (left panel) and without (right panel) c.m. momentum approximation are shown. The RBHF results are represented by open and solid circles, where open circles stand for the data used in the fit and solid circles indicate the validity of the results of the fit (solid curves). The red stars indicate the saturation points obtained from RBHF results.

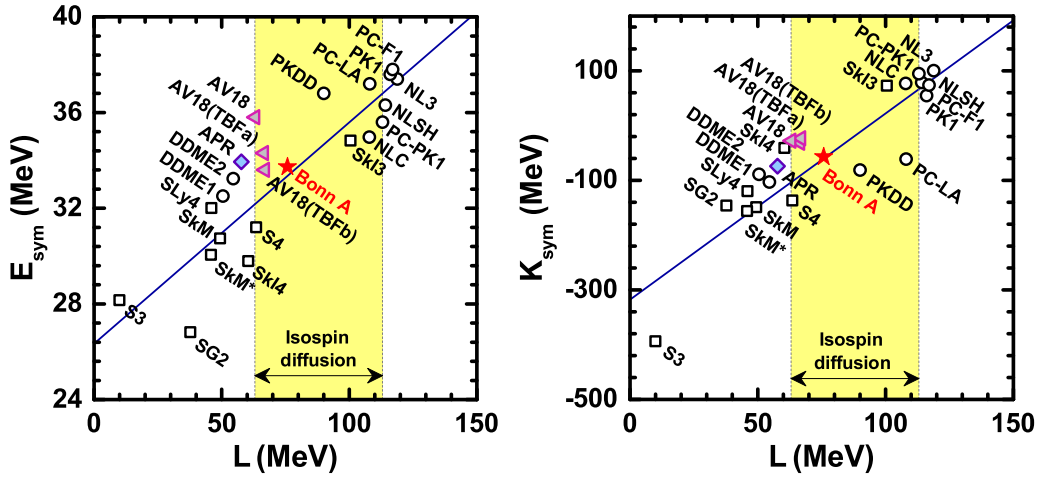

FIG. 2. $E_{\rm sym}$ (left panel) and $K_{\rm sym}$ (right panel) as a function of L calculated by RBHF theory using the potential Bonn A (red star), in comparison with results obtained by BHF (triangles) [72], variational methods (APR, diamond) [78], and various density functionals (circles and squares) [54,79]. The shaded regions denote the constraints on L from isospin diffusion [7,58,80]. The blue line is the linear fit to the results of density functionals.

region. It was shown by Sagawa *et al.* [54], that K_τ is largely negative and shows an anticorrelation with incompressibility of nuclear matter K_∞ for both nonrelativistic and relativistic density functionals; that is, any approach that has a larger K_∞ gives a smaller K_τ. The same conclusions have been verified in the microscopic calculations.

As noted previously in Eq. (12), the incompressibility K_A of finite nuclei may be parametrized as [53]

$$K_A \approx K_\infty + K_{\rm surf} A^{-1/3} + K_\tau \alpha^2 + K_{\rm Coul} \frac{Z^2}{A^{4/3}}. \qquad (35)$$

$K_{\rm Coul}$ is essentially a model-independent term (in the sense that the deviations from one theoretical model to another are quite small) [54]. Therefore, in order to obtain K_τ, an approximately quadratic relation between $K_A - K_{\rm Coul} Z^2 A^{-4/3}$ and the asymmetry parameter α can be used to fit the experimental data. In Refs. [75,82], a value of -5.2 ± 0.7 MeV was used for $K_{\rm Coul}$, derived from 13 parameter sets of the Skyrme interaction [54], and the uncertainty in the value of $K_{\rm Coul}$ contributes ∼15 MeV to K_τ for the measurement of the ISGMR in even-A Sn isotopes and ∼20 MeV in even-A Cd isotopes.

As discussed earlier, we can see in Fig. 4 that the values of $K_{\rm Coul}$ derived from RBHF theory using the Bonn potentials are larger than those derived from BHF because the skewness parameters Q_0 are large and positive for RBHF theory. In addition, the values of $K_{\rm Coul}$ provided by the relativistic approaches including RBHF are larger than -5.2 ± 0.7 MeV, which indicates that higher order corrections (e.g., Q_0) play an important role in $K_{\rm Coul}$. Therefore it is important to study the effects on K_τ derived from relativistic approaches when using different values of $K_{\rm Coul}$.

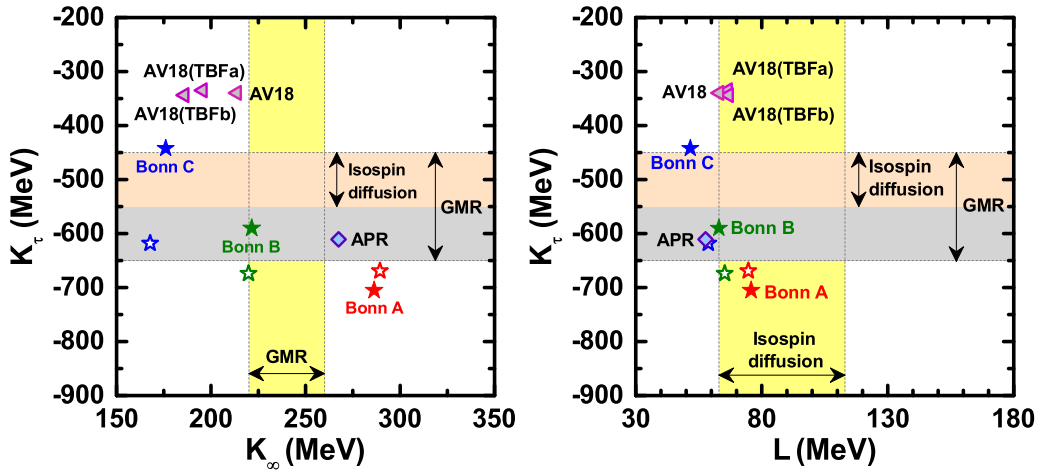

FIG. 3. Correlations between the parameters K_τ and K_∞ (left panel) and between K_τ and L (right panel) calculated by RBHF theory using the Bonn potentials with (open star) and without (solid star) averaged c.m. momentum approximation. The results are compared with BHF (triangles) [72] and with APR (diamond) [78]. The shaded regions indicate the experimental ranges of K_τ and K_∞ derived from from the ISGMR of Sn isotopes [56,75] and of K_τ and L determined in Refs. [7,58,80] from isospin diffusion.

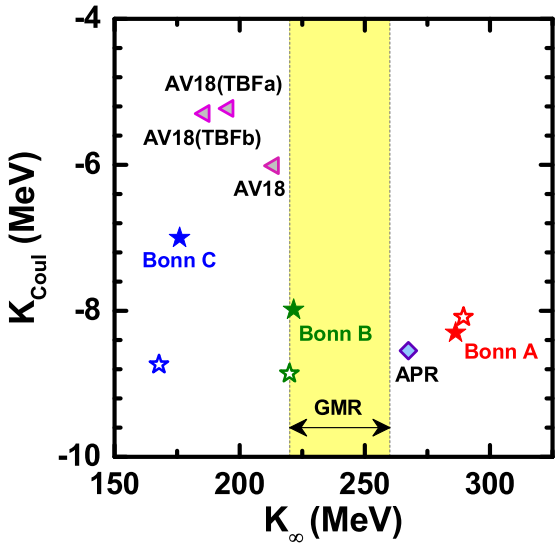

FIG. 4. Values of $K_{\rm Coul}$ and K_∞ calculated by RBHF theory using the Bonn potentials with (open star) and without (solid star) averaged c.m. momentum approximation, compared with BHF (triangles) [72] and APR (diamond) [78]. The shaded regions denote the constraints on K_∞ from the ISGMR of Sn isotopes [56,75].

IV. SUMMARY

Quantities like the binding energy of symmetric nuclear matter and the symmetry energy and their density dependence play an important role in modern nuclear physics and astrophysics. Nonrelativistic and relativistic Brueckner-Hartree-Fock theory allows an *ab initio* derivation of these quantities from the experimentally known bare nucleon-nucleon interaction. In the present paper, by employing the Fermi sphere method we derived an exact and analytic expression of the angular integrations for the c.m. momentum $\boldsymbol{P}$, which is important for a precise numerical calculation of the binding energy, especially for asymmetric nuclear matter. In order to examine the effect of the exact treatment of the c.m. momentum and to assess the reliability of the averaged c.m. momentum approximation, we have systematically studied the density dependence of the energy of symmetric nuclear matter and of the symmetry energy in the vicinity of the saturation density ρ_0, within relativistic Brueckner-Hartree-Fock theory using the Bonn potentials with and without averaged c.m. momentum approximation.

Our results clarified that for some of the properties, such as ρ_0, E/A, K_∞, $E_{\rm sym}$, and L, the approximation of an averaged c.m. momentum is quantitatively reliable, but for the remaining higher order parameters, such as Q_0, M_0, $K_{\rm sym}$, $K_{\rm asy}$, $K_{\rm Coul}$, and K_τ there are considerable discrepancies between the exact treatment of the angle integrations and the angle-averaged approximation.

Furthermore, the results of our relativistic calculations were compared with those of nonrelativistic BHF theory. It turns out that the saturation density ρ_0, the binding energy per particle E/A, and the incompressibility K_∞ derived from RBHF theory agree better with the empirical values than those from nonrelativistic BHF theory.

We have also studied the correlation between L and $E_{\rm sym}$ and L and $K_{\rm sym}$. It is found that the results of RBHF, BHF, and variational calculations (APR) are in excellent agreement with the tight correlations already obtained by other calculations using nonrelativistic and relativistic density functionals. This agreement suggests that these correlations are not only due to the mean field nature of these approaches but also exist in the microscopic methods. We have confirmed for the microscopic methods that there is an anticorrelation between the symmetry

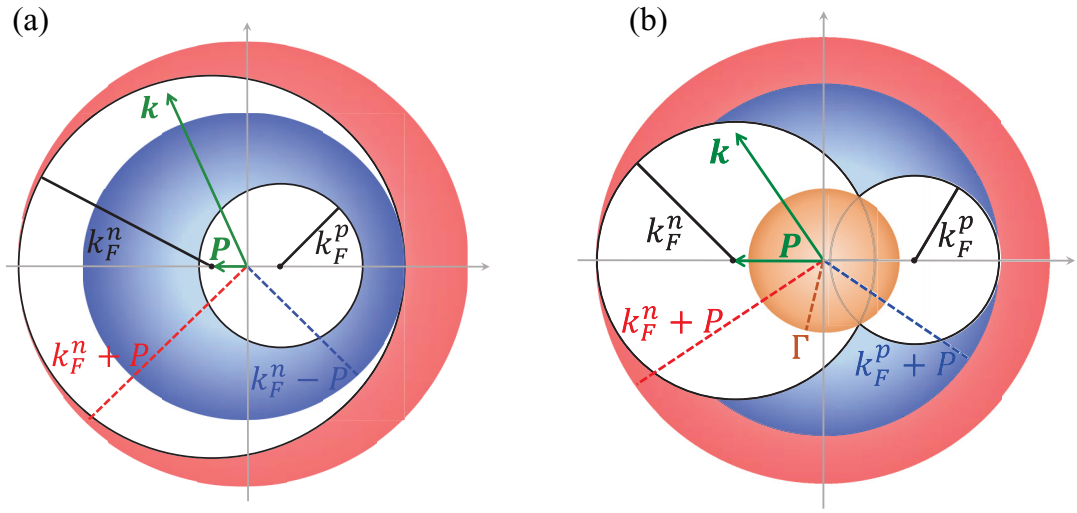

FIG. 5. Angle-averaged Pauli operator $Q_{np}^{\rm av}$ of a proton and neutron with two different Fermi momenta. Left panel (a): $(k_F^n - k_F^p)/2 \geqslant P \geqslant 0$. Right panel (b): $(k_F^n + k_F^p)/2 \geqslant P > (k_F^n - k_F^p)/2$. Green vector lines represent the c.m. momentum $\boldsymbol{P}$ and relative momentum $\boldsymbol{k}$. The maximum range of $|\boldsymbol{k}|$ for different parts are denoted by dashed lines, where $\Gamma = \sqrt{({k_F^n}^2 + {k_F^p}^2)/2 - P^2}$. For reference, the Fermi spheres of protons and neutrons are also given with two different Fermi momenta k_F^n, k_F^p.

term K_τ and the incompressibility K_∞, a trend pointed out by Sagawa *et al.* [54]. In addition, we note that the microscopic predictions for Q_0 from RBHF theory are large and positive, in contrast to nonrelativistic BHF theory, where one finds negative values. Our results indicate that generally the higher order Q_0 contribution to K_τ cannot be neglected, and that the value of the higher order corrections Q_0 play an important role for the evaluation of $K_{\rm Coul}$.

ACKNOWLEDGMENTS

This work was partly supported by the National Key R&D Program of China (2018YFA0404400), the National Natural Science Foundation of China (NSFC) under Grants No. 11335002, No. 11621131001, and No. 11775099, the China Postdoctoral Science Foundation under Grants No. 2016M600845 and No. 2017T100008, and the Deutsche Forschungsgemeinschaft (Germany) cluster of excellence "Origin and Structure of Universe" (www.universe-cluster.de).

APPENDIX A: ANGLE-AVERAGED PAULI OPERATOR

The definition of the angle-averaged Pauli operator is

$$Q^{\rm av}_{\tau_1\tau_2}(k,P)=\frac{\int Q_{\tau_1\tau_2}(\boldsymbol{k},\boldsymbol{P})d\Omega}{\int d\Omega}, \tag{A1}$$

where Ω is the angle between $\boldsymbol{k}$ and $\boldsymbol{P}$. In the following we concentrate on the case $\tau_1\neq\tau_2$. The case $\tau_1=\tau_2$ is simpler and can be derived in an analogous way. As usual we assume $k_F^n\geqslant k_F^p$. As shown in Fig. 5, we make use of two different Fermi spheres in momentum space representing protons and neutrons. They are displaced by $\pm\boldsymbol{P}$ relative to the origin. Taking the direction of the c.m. momentum $\boldsymbol{P}$ along the horizontal axis, then the solid angle $d\Omega$ is linked with the vector $\boldsymbol{k}$. Because of the Pauli exclusion principle the vectors $\boldsymbol{P}+\boldsymbol{k}$ and $\boldsymbol{P}-\boldsymbol{k}$ should be outside of the two solid black spheres. This leads to several different angular interval regions with different colors. We have to distinguish three cases, depending on the values of k, P, k_F^p, and k_F^n.

(a) $(k_F^n-k_F^p)/2\geqslant P\geqslant 0$:

$$Q^{\rm av}_{\tau_1\tau_2}(k,P)=\begin{cases}0, & k<k_F^n-P,\\ \frac{1}{2}\left(\frac{k^2+P^2-{k_F^n}^2}{2Pk}+1\right), & k_F^n-P\leqslant k<k_F^n+P,\\ 1, & k_F^n+P\leqslant k.\end{cases} \tag{A2}$$

(b) $(k_F^n+k_F^p)/2\geqslant P>(k_F^n-k_F^p)/2$:

$$Q^{\rm av}_{\tau_1\tau_2}(k,P)=\begin{cases}0, & k<\Gamma,\\ \frac{k^2-\Gamma^2}{2Pk}, & \Gamma\leqslant k<k_F^p+P,\\ \frac{1}{2}\left(\frac{k^2+P^2-{k_F^n}^2}{2Pk}+1\right), & k_F^p+P\leqslant k<k_F^n+P,\\ 1, & k_F^n+P\leqslant k.\end{cases} \tag{A3}$$

(c) $P>(k_F^n+k_F^p)/2$:

$$Q^{\rm av}_{\tau_1\tau_2}(k,P)=0. \tag{A4}$$

APPENDIX B: EXACT ANGULAR INTEGRATIONS FOR THE c.m. MOMENTUM IN EQ. (29)

We discuss here details of the angular integration for the evaluation of the potential energy in Eq. (29). As mentioned in Eqs. (31) and (32), we need to distinguish $k_F^n\leqslant 3k_F^p$ and $k_F^n\geqslant 3k_F^p$. There exists a critical condition of $k_F^n=3k_F^p$ shown in Fig. 6. Now we make use of two Fermi spheres in momentum space displaced by $\pm\boldsymbol{q}$ relative to the origin and $k_F^p=|\boldsymbol{q}|$. Here one finds the origin of coordinates (i.e., the midpoint between the two center points of the two Fermi spheres) on the boundary of the red circle, and the two Fermi spheres are perfectly tangent at the same time. According to Eq. (29) only occupied states, i.e., only momenta with $|\boldsymbol{k}_m|=|\boldsymbol{P}+\boldsymbol{q}|\leqslant k_F^p$ and $|\boldsymbol{k}_n|=|\boldsymbol{P}-\boldsymbol{q}|\leqslant k_F^n$ in the red region, contribute to the integration $\int d\Omega_P=\int\sin\theta\,d\theta\,d\phi$. Therefore the angular integrations can be calculated as

$$\int d\Omega_P=\int_0^{2\pi}d\phi\int_0^{\theta_0}\sin\theta\,d\theta=-2\pi\int_0^{\theta_0}d\cos\theta. \tag{B1}$$

Using the cosine law

$$\cos\theta_0=-\frac{{k_F^p}^2-q^2-P^2}{2qP}, \tag{B2}$$

the final result of this special case is obtained as

$$\int d\Omega_P=2\pi\left(1+\frac{{k_F^p}^2-q^2-P^2}{2qP}\right)\quad\text{for}\quad 0\leqslant P\leqslant 2k_F^p. \tag{B3}$$

For the cases $k_F^p\leqslant|\boldsymbol{q}|$ and $k_F^p\geqslant|\boldsymbol{q}|$, even though they are more complex, a similar analysis can be done. As we can see, considering the case of $k_F^n=3k_F^p$, one only needs to compare the values of k_F^p and $|\boldsymbol{q}|$. However, when extending to the case of $k_F^n\leqslant 3k_F^p$ and $k_F^n\geqslant 3k_F^p$, we should compare the values between $|\boldsymbol{q}|$ and k_F^p, $(k_F^n-k_F^p)/2$, $(k_F^n+k_F^p)/2$, as shown in the following formulas (B5)–(B10).

Here we first give an example shown in Fig. 7 for the case of $k_F^n\leqslant 3k_F^p$, $k_F^p\geqslant|\boldsymbol{q}|>(k_F^n-k_F^p)/2$. We make use of two different Fermi spheres in momentum space to represent protons and neutrons, displaced by $\pm\boldsymbol{q}$ relative to the origin. Taking the direction of the relative momentum $\boldsymbol{q}$ along the horizontal axis, the solid angle $d\Omega_P$ is linked with the vector $\boldsymbol{P}$. Considering the integration of the ground state energy in

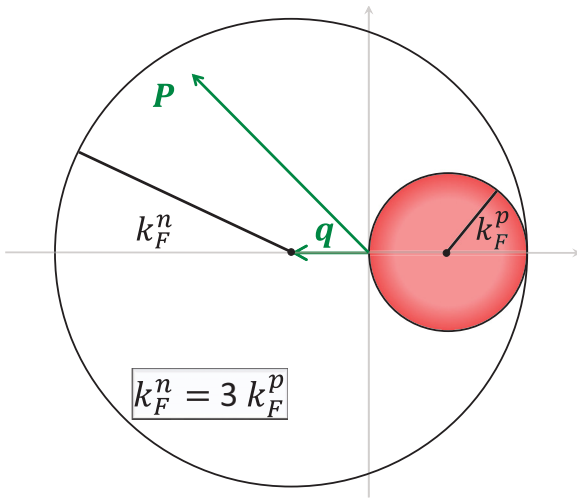

FIG. 6. The c.m. momentum angular integrations in the case of $k_F^n = 3k_F^p$, $k_F^p = |\boldsymbol{q}|$. Only the red region contributes to the integral.

Eq. (29), the vectors $\boldsymbol{P}+\boldsymbol{q}=\boldsymbol{k_m}$ and $\boldsymbol{P}-\boldsymbol{q}=\boldsymbol{k_n}$ should be inside the two solid black Fermi spheres with the radii k_F^n and k_F^p. This is possible in three different angular intervals with different colors (orange, blue, and red). The maximum range of $|\boldsymbol{P}|$ for the three different parts is represented as $k_F^p - q$, $k_F^n - q$, and $\Gamma = [\frac{1}{2}({k_F^n}^2 + {k_F^p}^2) - q^2]^{1/2}$, respectively.

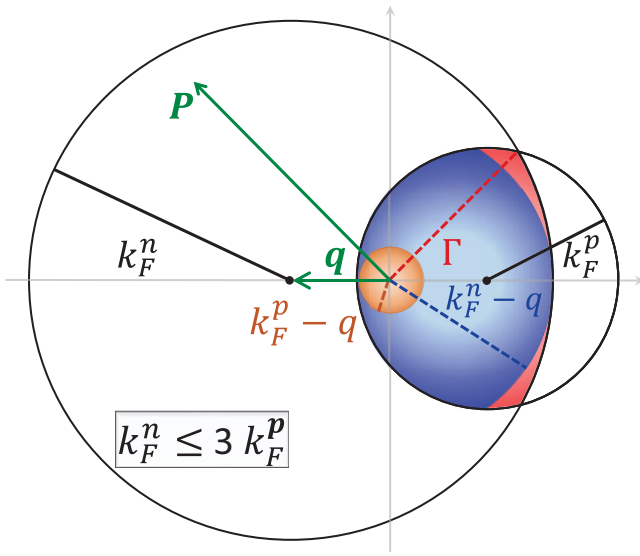

FIG. 7. Different regions contributing to the c.m. momentum angular integrations in the case of $k_F^n \leqslant 3k_F^p$, $k_F^p \geqslant |\boldsymbol{q}| > (k_F^n - k_F^p)/2$. Only the overlap (orange, blue, and red) contributes to the integral. The orange, blue, and red regions denote three angular intervals of integration, which separate the whole space into four parts as given in Eq. (B4). Green vector lines represent the c.m. momentum $\boldsymbol{P}$ and relative momentum $\boldsymbol{q}$. The maximum range of $|\boldsymbol{P}|$ for three different parts are denoted by dashed lines. For reference, the Fermi spheres of protons and neutrons are also given with two different Fermi momentum k_F^n, k_F^p.

Finally we have

$$\int d\Omega_P = \begin{cases} 4\pi, & 0 \leqslant P \leqslant k_F^p - q, \\ 2\pi\left(1 + \frac{k_F^{p\,2} - q^2 - P^2}{2qP}\right), & k_F^p - q < P \leqslant k_F^n - q, \\ 2\pi\left(\frac{\Gamma^2 - P^2}{qP}\right), & k_F^n - q < P \leqslant \Gamma, \\ 0, & \Gamma < P. \end{cases} \tag{B4}$$

In a more general case we have the following possibilities.

1. $k_F^n \geqslant 3k_F^p$

(a) $0 \leqslant q \leqslant k_F^p$:

$$\int d\Omega_P = \begin{cases} 4\pi, & 0 \leqslant P \leqslant k_F^p - q, \\ 2\pi\left(1 + \frac{k_F^{p\,2} - q^2 - P^2}{2qP}\right), & k_F^p - q < P \leqslant k_F^p + q. \end{cases} \tag{B5}$$

(b) $k_F^p < q \leqslant (k_F^n - k_F^p)/2$:

$$\int d\Omega_P = 2\pi\left(1 + \frac{k_F^{p\,2} - q^2 - P^2}{2qP}\right), \quad q - k_F^p \leqslant P \leqslant q + k_F^p. \tag{B6}$$

(c). $(k_F^n - k_F^p)/2 < q \leqslant (k_F^n + k_F^p)/2$

$$\int d\Omega_P = \begin{cases} 2\pi\left(1 + \frac{k_F^{p\,2} - q^2 - P^2}{2qP}\right), & q - k_F^p \leqslant P \leqslant k_F^n - q \\ 2\pi\left(\frac{\Gamma^2 - P^2}{qP}\right), & k_F^n - q < P \leqslant \Gamma. \end{cases} \tag{B7}$$

2. $k_F^n \leqslant 3k_F^p$

(a) $0 \leqslant q \leqslant (k_F^n - k_F^p)/2$:

$$\int d\Omega_P = \begin{cases} 4\pi, & 0 \leqslant P \leqslant k_F^p - q, \\ 2\pi\left(1 + \frac{k_F^{p\,2} - q^2 - P^2}{2qP}\right), & k_F^p - q < P \leqslant k_F^p + q. \end{cases} \tag{B8}$$

(b) $(k_F^n - k_F^p)/2 < q \leqslant k_F^p$:

$$\int d\Omega_P = \begin{cases} 4\pi, & 0 \leqslant P \leqslant k_F^p - q, \\ 2\pi\left(1 + \frac{k_F^{p\,2} - q^2 - P^2}{2qP}\right), & k_F^p - q < P \leqslant k_F^n - q, \\ 2\pi\left(\frac{\Gamma^2 - P^2}{qP}\right), & k_F^n - q < P \leqslant \Gamma. \end{cases} \tag{B9}$$

(c) $k_F^p < q \leqslant (k_F^n + k_F^p)/2$:

$$\int d\Omega_P = \begin{cases} 2\pi\left(1 + \frac{k_F^{p\,2} - q^2 - P^2}{2qP}\right), & q - k_F^p \leqslant P \leqslant k_F^n - q, \\ 2\pi\left(\frac{\Gamma^2 - P^2}{qP}\right), & k_F^n - q < P \leqslant \Gamma. \end{cases} \tag{B10}$$

APPENDIX C: AVERAGED CENTER-OF-MASS MOMENTUM

The definition of the average c.m. momentum is given in Ref. [48]:

$$P_{\rm av}^2 = \frac{\int_0^{k_F^n} d^3k_1 \int_0^{k_F^p} d^3k_2 P^2 \delta\left(q - \frac{1}{2}|\boldsymbol{k}_1 - \boldsymbol{k}_2|\right)}{\int_0^{k_F^n} d^3k_1 \int_0^{k_F^p} d^3k_2 \delta\left(q - \frac{1}{2}|\boldsymbol{k}_1 - \boldsymbol{k}_2|\right)}. \tag{C1}$$

To simplify the final expressions, we introduce in the integral the following notations:

$$x = k_F^n + q, \quad y = k_F^p - q, \quad s = k_F^n - q, \quad t = k_F^p + q. \tag{C2}$$

The final expressions are as follows.

1. $k_F^n \geqslant 3k_F^p$

$$P_{\rm av}^2 = \begin{cases} \frac{3}{5}\left(k_F^p\right)^2 + q^2, & 0 \leqslant q \leqslant k_F^p, \\ \frac{\frac{8}{5}qs^5 + yt^5 + sxt^4 - s^5x + \frac{2}{3}s^6 - \frac{4}{3}t^6}{\frac{8}{3}qs^3 + 2yt^3 + 2sxt^2 - 2s^3x + s^4 - 2t^4}, & k_F^p < q \leqslant \left(k_F^n - k_F^p\right)/2, \\ \frac{\frac{8}{5}q(s^5+y^5) + \frac{1}{12}(ty+sx)^3 + \frac{2}{3}(s^6+y^6) - (ty^5+xs^5)}{\frac{8}{3}q(s^3+y^3) + \frac{1}{2}(ty+sx)^2 + (s^4+y^4) - 2(ty^3+xs^3)}, & \left(k_F^n - k_F^p\right)/2 < q \leqslant \left(k_F^n + k_F^p\right)/2, \\ 0, & \left(k_F^n + k_F^p\right)/2 < q. \end{cases} \tag{C3}$$

2. $k_F^n \leqslant 3k_F^p$

$$P_{\rm av}^2 = \begin{cases} \frac{3}{5}\left(k_F^p\right)^2 + q^2, & 0 \leqslant q \leqslant \left(k_F^n - k_F^p\right)/2, \\ \frac{\frac{8}{5}q(s^5+y^5) + \frac{1}{12}(ty+sx)^3 + \frac{2}{3}(s^6+y^6) - (ty^5+xs^5)}{\frac{8}{3}q(s^3+y^3) + \frac{1}{2}(ty+sx)^2 + (s^4+y^4) - 2(ty^3+xs^3)}, & \left(k_F^n - k_F^p\right)/2 < q \leqslant \left(k_F^n + k_F^p\right)/2, \\ 0, & \left(k_F^n + k_F^p\right)/2 < q. \end{cases} \tag{C4}$$

[1] J. M. Lattimer and M. Prakash, Phys. Rep. **333-334**, 121 (2000).
[2] B. A. Brown, Phys. Rev. Lett. **85**, 5296 (2000).
[3] P. Danielewicz, R. Lacey, and W. G. Lynch, Science **298**, 1592 (2002).
[4] J. M. Lattimer and M. Prakash, Science **304**, 536 (2004).
[5] A. W. Steiner, M. Prakash, J. M. Lattimer, and P. J. Ellis, Phys. Rep. **411**, 325 (2005).
[6] V. Baran, M. Colonna, V. Greco, and M. Di Toro, Phys. Rep. **410**, 335 (2005).
[7] B.-A. Li, L.-W. Chen, and C. M. Ko, Phys. Rep. **464**, 113 (2008).
[8] M. Centelles, X. Roca-Maza, X. Viñas, and M. Warda, Phys. Rev. Lett. **102**, 122502 (2009).
[9] T. H. R. Skyrme, Philos. Mag. **1**, 1043 (1956).
[10] D. Vautherin and D. M. Brink, Phys. Rev. C **5**, 626 (1972).
[11] J. Dechargé and D. Gogny, Phys. Rev. C **21**, 1568 (1980).
[12] J. Boguta and A. R. Bodmer, Nucl. Phys. A **292**, 413 (1977).
[13] P. G. Reinhard, Rep. Prog. Phys. **52**, 439 (1989).
[14] P. Ring, Prog. Part. Nucl. Phys. **37**, 193 (1996).
[15] J. Meng, H. Toki, S. G. Zhou, S. Q. Zhang, W. H. Long, and L. S. Geng, Prog. Part. Nucl. Phys. **57**, 470 (2006).
[16] J. Meng, *Relativistic Density Functional for Nuclear Structure* (World Scientific, Singapore, 2016).
[17] R. Machleidt, Adv. Nucl. Phys. **19**, 189 (1989).
[18] R. B. Wiringa, V. G. J. Stoks, and R. Schiavilla, Phys. Rev. C **51**, 38 (1995).
[19] R. Machleidt, Phys. Rev. C **63**, 024001 (2001).
[20] P. F. Bedaque and U. van Kolck, Annu. Rev. Nucl. Part. Sci. **52**, 339 (2002).
[21] E. Epelbaum, H.-W. Hammer, and U.-G. Meißner, Rev. Mod. Phys. **81**, 1773 (2009).
[22] R. Machleidt and D. Entem, Phys. Rep. **503**, 1 (2011).
[23] X.-L. Ren, K.-W. Li, L.-S. Geng, B. Long, P. Ring, and J. Meng, Chin. Phys. C **42**, 014103 (2018).
[24] J. Carlson, S. Gandolfi, F. Pederiva, S. C. Pieper, R. Schiavilla, K. E. Schmidt, and R. B. Wiringa, Rev. Mod. Phys. **87**, 1067 (2015).
[25] G. Hagen, T. Papenbrock, M. Hjorth-Jensen, and D. J. Dean, Rep. Prog. Phys. **77**, 096302 (2014).
[26] B. R. Barrett, P. Navràtil, and J. P. Vary, Prog. Part. Nucl. Phys. **69**, 131 (2013).
[27] W. Dickhoff and C. Barbieri, Prog. Part. Nucl. Phys. **52**, 377 (2004).
[28] D. Lee, Prog. Part. Nucl. Phys. **63**, 117 (2009).
[29] H. Hergert, S. Bogner, T. Morris, A. Schwenk, and K. Tsukiyama, Phys. Rep. **621**, 165 (2016).
[30] T. Otsuka, M. Honma, T. Mizusaki, N. Shimizu, and Y. Utsuno, Prog. Part. Nucl. Phys. **47**, 319 (2001).
[31] L. Liu, T. Otsuka, N. Shimizu, Y. Utsuno, and R. Roth, Phys. Rev. C **86**, 014302 (2012).
[32] B. D. Day, Rev. Mod. Phys. **39**, 719 (1967).
[33] M. Anastasio, L. Celenza, W. Pong, and C. Shakin, Phys. Rep. **100**, 327 (1983).
[34] C. Horowitz and B. D. Serot, Phys. Lett. B **137**, 287 (1984).

[35] R. Brockmann and R. Machleidt, Phys. Rev. C **42**, 1965 (1990).
[36] G. Q. Li, R. Machleidt, and R. Brockmann, Phys. Rev. C **45**, 2782 (1992).
[37] L. Engvik, M. Hjorth-Jensen, E. Osnes, G. Bao, and E. Østgaard, Phys. Rev. Lett. **73**, 2650 (1994).
[38] L. Sehn, C. Fuchs, and A. Faessler, Phys. Rev. C **56**, 216 (1997).
[39] F. de Jong and H. Lenske, Phys. Rev. C **57**, 3099 (1998).
[40] D. Alonso and F. Sammarruca, Phys. Rev. C **67**, 054301 (2003).
[41] E. N. E. van Dalen, C. Fuchs, and A. Faessler, Phys. Rev. Lett. **95**, 022302 (2005).
[42] T. Katayama and K. Saito, Phys. Rev. C **88**, 035805 (2013).
[43] S.-H. Shen, J.-N. Hu, H.-Z. Liang, J. Meng, P. Ring, and S.-Q. Zhang, Chin. Phys. Lett. **33**, 102103 (2016).
[44] S. Shen, H. Liang, J. Meng, P. Ring, and S. Zhang, Phys. Rev. C **96**, 014316 (2017).
[45] S. Shen, H. Liang, J. Meng, P. Ring, and S. Zhang, Phys. Lett. B **778**, 344 (2018).
[46] S. Shen, H. Liang, J. Meng, P. Ring, and S. Zhang, Phys. Lett. B **781**, 227 (2018).
[47] S. Shen, H. Liang, J. Meng, P. Ring, and S. Zhang, Phys. Rev. C **97**, 054312 (2018).
[48] K. A. Brueckner, S. A. Coon, and J. Dabrowski, Phys. Rev. **168**, 1184 (1968).
[49] F. Sammarruca, B. Chen, L. Coraggio, N. Itaco, and R. Machleidt, Phys. Rev. C **86**, 054317 (2012).
[50] F. Sammarruca, Eur. Phys. J. A **50**, 22 (2014).
[51] N. Alam, B. K. Agrawal, J. N. De, S. K. Samaddar, and G. Colò, Phys. Rev. C **90**, 054317 (2014).
[52] N. Alam, B. K. Agrawal, M. Fortin, H. Pais, C. Providência, A. R. Raduta, and A. Sulaksono, Phys. Rev. C **94**, 052801 (2016).
[53] J. P. Blaizot, Phys. Rep. **64**, 171 (1980).
[54] H. Sagawa, S. Yoshida, G.-M. Zeng, J.-Z. Gu, and X.-Z. Zhang, Phys. Rev. C **76**, 034327 (2007).
[55] G. Colò, U. Garg, and H. Sagawa, Eur. Phys. J. A **50**, 26 (2014).
[56] U. Garg and G. Colò, Prog. Part. Nucl. Phys. **101**, 55 (2018).
[57] S. F. Ban, J. Li, S. Q. Zhang, H. Y. Jia, J. P. Sang, and J. Meng, Phys. Rev. C **69**, 045805 (2004).
[58] L.-W. Chen, C. M. Ko, and B.-A. Li, Phys. Rev. Lett. **94**, 032701 (2005).
[59] S. Ban, J. Meng, W. Satuła, and R. A. Wyss, Phys. Lett. B **633**, 231 (2006).
[60] B. Y. Sun, W. H. Long, J. Meng, and U. Lombardo, Phys. Rev. C **78**, 065805 (2008).
[61] R. H. Thompson, Phys. Rev. D **1**, 110 (1970).
[62] E. E. Salpeter and H. A. Bethe, Phys. Rev. **84**, 1232 (1951).
[63] B. D. Serot and J. D. Walecka, Adv. Nucl. Phys. **16**, 1 (1986).
[64] E. Schiller, H. Müther, and P. Czerski, Phys. Rev. C **59**, 2934 (1999).
[65] E. Schiller, H. Müther, and P. Czerski, Phys. Rev. C **60**, 059901(E) (1999).
[66] K. Suzuki, R. Okamoto, M. Kohno, and S. Nagata, Nucl. Phys. A **665**, 92 (2000).
[67] J. P. Jeukenne, A. Lejeune, and C. Mahaux, Phys. Rep. **25**, 83 (1976).
[68] M. Baldo, I. Bombaci, L. S. Ferreira, G. Giansiracusa, and U. Lombardo, Phys. Rev. C **43**, 2605 (1991).
[69] C. Drischler, V. Somà, and A. Schwenk, Phys. Rev. C **89**, 025806 (2014).
[70] H. A. Bethe, Annu. Rev. Nucl. Sci. **21**, 93 (1971).
[71] D. W. L. Sprung, Adv. Nucl. Phys. **5**, 225 (1972).
[72] I. Vidaña, C. Providência, A. Polls, and A. Rios, Phys. Rev. C **80**, 045806 (2009).
[73] M. Baldo and L. S. Ferreira, Phys. Rev. C **59**, 682 (1999).
[74] Z. H. Li, U. Lombardo, H.-J. Schulze, W. Zuo, L. W. Chen, and H. R. Ma, Phys. Rev. C **74**, 047304 (2006).
[75] T. Li *et al.*, Phys. Rev. Lett. **99**, 162503 (2007).
[76] U. Garg *et al.*, Nucl. Phys. A **788**, 36 (2007).
[77] S. Gandolfi, J. Carlson, and S. Reddy, Phys. Rev. C **85**, 032801 (2012).
[78] A. Akmal, V. R. Pandharipande, and D. G. Ravenhall, Phys. Rev. C **58**, 1804 (1998).
[79] P. W. Zhao, Z. P. Li, J. M. Yao, and J. Meng, Phys. Rev. C **82**, 054319 (2010).
[80] L.-W. Chen, C. M. Ko, and B.-A. Li, Phys. Rev. C **72**, 064309 (2005).
[81] L.-W. Chen, B.-J. Cai, C. M. Ko, B.-A. Li, C. Shen, and J. Xu, Phys. Rev. C **80**, 014322 (2009).
[82] D. Patel *et al.*, Phys. Lett. B **718**, 447 (2012).